Bioprinting 22 (2021) e00133

Contents lists available at ScienceDirect

Bioprinting

journal homepage: www.elsevier.com/locate/bprint

3D printed, mechanically tunable, composite sodium alginate, gelatin and Gum Arabic (SA-GEL-GA) scaffolds

Mahmoud Amr [b], India Dykes [c], Michele Counts [e], Joshua Kernan [a], Alia Mallah [b], Juana Mendenhall [d], Bernard Van Wie [c], Nehal Abu-Lail [b], B. Arda Gozen [a,*]

[a] Washington State University, School of Mechanical and Materials Engineering, United States
[b] University of Texas-San Antonio, Department of Biomedical Engineering and Chemical Engineering, United States
[c] Washington State University, Voiland School of Chemical and Bioengineering, United States
[d] Morehouse College, Department of Chemistry, United States
[e] University of Rochester, Department of Biomedical Engineering, United States

ARTICLE INFO

Keywords:
3D bioprinting
Additive manufacturing
Bioink
Hydrogel
Tissue engineering
Rheology

ABSTRACT

Biomimicking the mechanical properties of native tissues is one of the key requirements of engineering tissue scaffolds, rendering a need for materials and manufacturing processes with a high level of control over the mechanical properties of such scaffolds. To address this need, we present a 3D printable, composite hydrogel consisting of sodium alginate (SA), gelatin (GEL) and gum Arabic (GA), referred to herein as SA-GEL-GA hydrogel, mechanical properties of which can be controlled through tuning its cross-linking process. Here, the aqueous solution of the three constituents is used as the bioink to 3D print porous scaffolds in a temperature-controlled extrusion-based printing process. 3D-printed scaffolds are then crosslinked through a multi-step approach, realizing the gelation of GEL, ionic crosslinking of SA and GA, and covalent cross-linking of all three components. Here, we show that the inherent mechanical properties of SA-GEL-GA hydrogels can be controlled through the duration of the covalent crosslinking step. SA-GEL-GA bioinks exhibit highly temperature-dependent rheology with elastic solid-like behavior below room temperature and a viscoplastic, shear thinning nature above 28 °C. Using a cooled build-plate and heated printhead, high resolution scaffolds were printed with filament diameter of 250 μm and extruded from a 100 μm diameter nozzle. The compressive elastic modulus of these scaffolds can be tuned to the 50–250 kPa range through the combined effect of the scaffold pores size and covalent crosslinking step duration. 3D printed and crosslinked scaffolds carry over 500% of their dry weight in water and can be dried and reswollen to over 400% of their dry weight. Finally, our degradation analysis showed that increased covalent cross-linking duration led to reduced long-term structural stability due to mechanical failure of the scaffolds. These results indicate that SA-GEL-GA hydrogels offer exciting opportunities for manufacturing customizable artificial tissue scaffolds with biomimicking mechanical properties, particularly for soft tissues.

1. Introduction

Bioprinting refers to additive manufacturing processes using biomaterials such as biopolymers, cells, growth factors etc. To fabricate living products including tissues and organs. Recently, these processes have drawn significant attention and global investment since they are considered one of the critical pieces for personalized medicine [1]. Among several bioprinting methods, extrusion-based approaches are the most widely used due to their broad range of material capabilities, low cost, and versatility. In extrusion-based bioprinting, "bioinks" consisting of hydrogels or water-soluble polymers that carry various biomaterials are dispensed out of nozzles and deposited in a layer-by-layer fashion, enabling fabrication of highly complex, multi-material structures [2]. These structures are often used as "scaffolds" that provide embedded cells with the proper support and environment for proliferation, growth and/or differentiation during cell culture, thereby constituting the initial step of the tissue manufacturing process. The success of this method in facilitating manufacturing of functional tissues relies heavily on how well the fabricated structures mimic the native tissues in terms of biomaterial organization and physical properties. As such, there is a significant need for research on processes and materials to advance the capabilities of extrusion-based bioprinting towards accurate and precise control of

* Corresponding author.
E-mail address: arda.gozen@wsu.edu (B.A. Gozen).

https://doi.org/10.1016/j.bprint.2021.e00133
Received 24 December 2020; Received in revised form 21 February 2021; Accepted 10 March 2021

printed structure properties within ranges relevant to native tissues.

Mechanical properties are among the most critical aspects of the native tissues that the biomanufacturing processes need to mimic effectively. Tissues in the human body exhibit a broad range of mechanical properties with elastic moduli ranging from hundreds of kPa for skin [3,4] to tens of GPa for bones [5]. Furthermore, most tissues are heterogeneous and anisotropic, exhibiting spatially varying mechanical properties such as tensile and shear moduli [6]. Precise control of the mechanical properties of the cell microenvironment is essential as this strongly influences resulting cellular physiological functions, communication, differentiation and proliferation [7,8].

Additive manufacturing (AM) using multiple materials can be used to fabricate composite structures with mechanical properties spatially tuned through distribution and morphology of different materials [9]. This approach has been particularly used in tissue engineering applications and primarily involves printing of high modulus "reinforcements", in the form of a scaffold consisting of extruded filaments, supporting a low modulus, cell-carrying hydrogel matrix [10,11]. The reinforcement materials are usually selected from rigid thermoplastic polymers [10–13] or polylactic acid (PLA) [14], which are significantly stiffer than hydrogels in general, or nanocomposites combining hydrogels with stiff additives to increase inherent stiffness along with printability [15–17]. Mechanical properties, specifically elastic modulus, are tuned through the reinforcing filament diameter and distribution, i.e. filament spacing and pattern [17,18]. These approaches combined with rational design and computational mechanics tools provide the opportunity to tune scaffold mechanical properties in a spatially varying fashion [19,20]. Despite these advances, several limitations still exist in bioprinting technologies for mechanical property control of engineered tissue scaffolds. First, the stiff thermoplastic polymers used for structural scaffold fabrication are generally printed in a completely molten phase at temperatures above 70 °C [12,17,21] using fused-deposition type printheads or through electrospinning methods under the effect of large electrical field [13,22]. This is unlike most cell-laden matrix hydrogels that are printed near room temperature using time-pressure dispensing from syringe-type printheads. Effectively printing these two types of materials simultaneously within highly resolved layers becomes challenging [10,21] due to thermally- and electrically-induced cell-viability concerns and precision engineering challenges emanating from contrast between the two types of printheads and multiple printing temperatures. This challenge, in turn, significantly limits scaffolds' designs, preventing precise control of not only the mechanical properties but also other critical aspects including cell-density and distribution within scaffolds. Secondly, inherent mechanical properties of the commonly used structural scaffold materials are limited to a narrow window that is significantly stiffer than matrix hydrogels used in tissue engineering applications. Furthermore, control of these properties is quite challenging as they depend on many complex and difficult-to-control process parameters influencing microstructure such as material cooling rates. For these materials, the only degrees of freedom to dictate the mechanical properties are the size and distribution of the structural scaffold filaments, which are insufficient for replicating the complex mechanical behavior of native tissues. To address these limitations, there is a pervasive need for new materials with inherently tunable properties and compatibility with cell-laden hydrogels as advances in bioprinting processes to realize additive manufacturing with such materials.

Towards realizing this advancement, this paper introduces a new composite hydrogel bioink formulation consisting of three natural polymeric components, sodium alginate (SA), gelatin (GEL) and Gum Arabic (GA), referred to here as SA-GEL-GA, as a promising structural scaffold material. This approach synergistically combines three constituents that are commonly used in tissue engineering and bioprinting applications. In that, it builds upon the previously reported results by Shi et al. [23] and Li et al. [24] indicating that the properties of the SA-GEL and SA-GA composites vary as a function of their crosslinking process, respectively. We aim to combine these three components in SA-GEL-GA to amplify these variations and utilize them to tune the mechanical properties of the 3D printed scaffolds.

SA-GEL-GA is printed using temperature-controlled extrusion-based printheads and cross-linked through a three-step process starting with physical crosslinking of GEL on chilled substrates, followed by duration-controlled ionic cross-linking of SA and GA [24] and covalent cross-linking of GEL [23] to obtain structures with desired final mechanical properties. The schematic representation of the chemical structure of the SA-GEL-GA hydrogels as illustrated in Fig. 1. In this work, we (1) report on the unique temperature-dependent hydrogel rheology, and its implications on bioprinting process, (2) investigate the effects of cross-linking durations and 3D printed scaffold geometry on the compressive moduli of the printed structures and (3) evaluate the utility of SA-GEL-GA for tissue engineering applications by studying its rehydration kinetics, and degradation. SA-GEL-GA hydrogel offers a clear advancement over conventional materials for bioprinting of structural tissue scaffolds with desired mechanical properties: Its unique temperature dependent rheology promotes printability using nozzles with diameters as small as 100 μm, thus improving resolution over the current state of the art in extrusion based bioprinting, while its cross-linking-dependent inherent mechanical properties offer an additional degree of freedom in mechanical property control towards achieving biomimicking scaffolds.

2. Materials and methods

2.1. Materials

The following materials were purchased from Sigma Aldrich (St. Louis, MO, USA): Gelatin from porcine skin, gel strength 300, type A (cat#: G2500), Alginic Acid, Sodium Salt (Sodium Alginate) (cat#: 180947), Gum Arabic from Acacia Tree (cat#: G9752), N-Hydroxysuccinimide (NHS) (cat#: 130672), N-(3-Dimethylaminopropyl)-N′-ethylcarbodiimide hydrochloride (EDC) (cat#: E7750), Calcium Chloride Anhydrous ($CaCl_2$) (cat#: C1016), 4-(2-Hydroxyethyl)piperazine-1-ethanesulfonic acid, N-(2-Hydroxyethyl)piperazine-N′-(2-ethanesulfonic acid) (HEPES) (cat#: H4034), and Dulbecco's Phosphate Buffered Saline (PBS) (cat#: D8662), Antibiotic Antimycotic (cat#: A5955). Dulbecco's Modified Eagle's Medium F12 + Glutamax (DMEM/F12) (cat#: 11965167) was purchased from Life Technologies Corp (Waltham, MA, USA).

2.2. Preparation of hydrogels

A known volume of deionized water (DIW) was pre-heated on a hotplate to a temperature of 50 °C. Sodium Alginate (SA), Gelatin (GEL), and Gum Arabic (GA) were then dissolved at concentrations of 5%, 10%, and 5% w/w respectively through continuous mixing with a high-speed mechanical stirrer (Cole-Parmer Compact Digital Mixer System), at a speed of 1000 rpm for 30 min. The hydrogel was loaded into sealed 60 ml syringes for long term storage, and transferred to 3 ml syringes for 3D printing.

2.3. Rheological characterization of hydrogels

Rheology of the hydrogels was characterized at different temperatures using a TA Instruments ARES-G2 rheometer (New Castle, DE, USA), equipped with an Advanced Peltier System (APS) using a 50 mm diameter cone and plate geometry. An oscillatory temperature sweep test was performed to study the variation of elastic and loss moduli as a function of temperature. The temperature was varied between 10 and 60 °C at an increasing rate of 5 °C/min while the sample was oscillated at a frequency of 1 rad/s with a strain amplitude of 1%. The moduli data were acquired at a rate of 1 Hz during this test. To understand the yield behavior of the hydrogels, oscillatory amplitude sweep tests were performed at 5 °C, 9 °C, 35 °C and 55 °C where the strain amplitude was

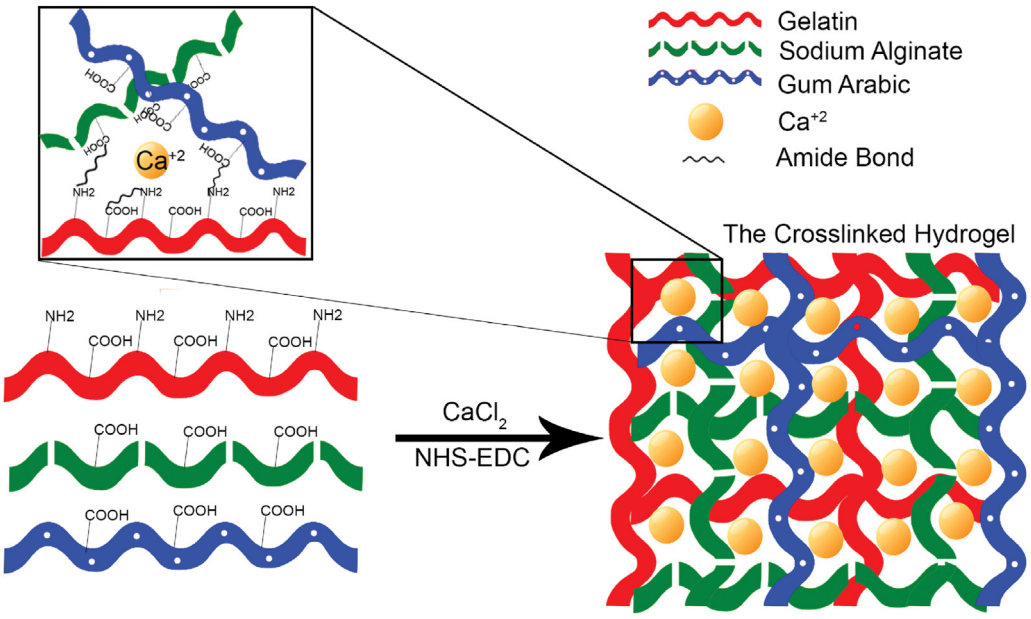

Fig. 1. Schematic representation of the chemical structure of the SA-GEL-GA hydrogel.

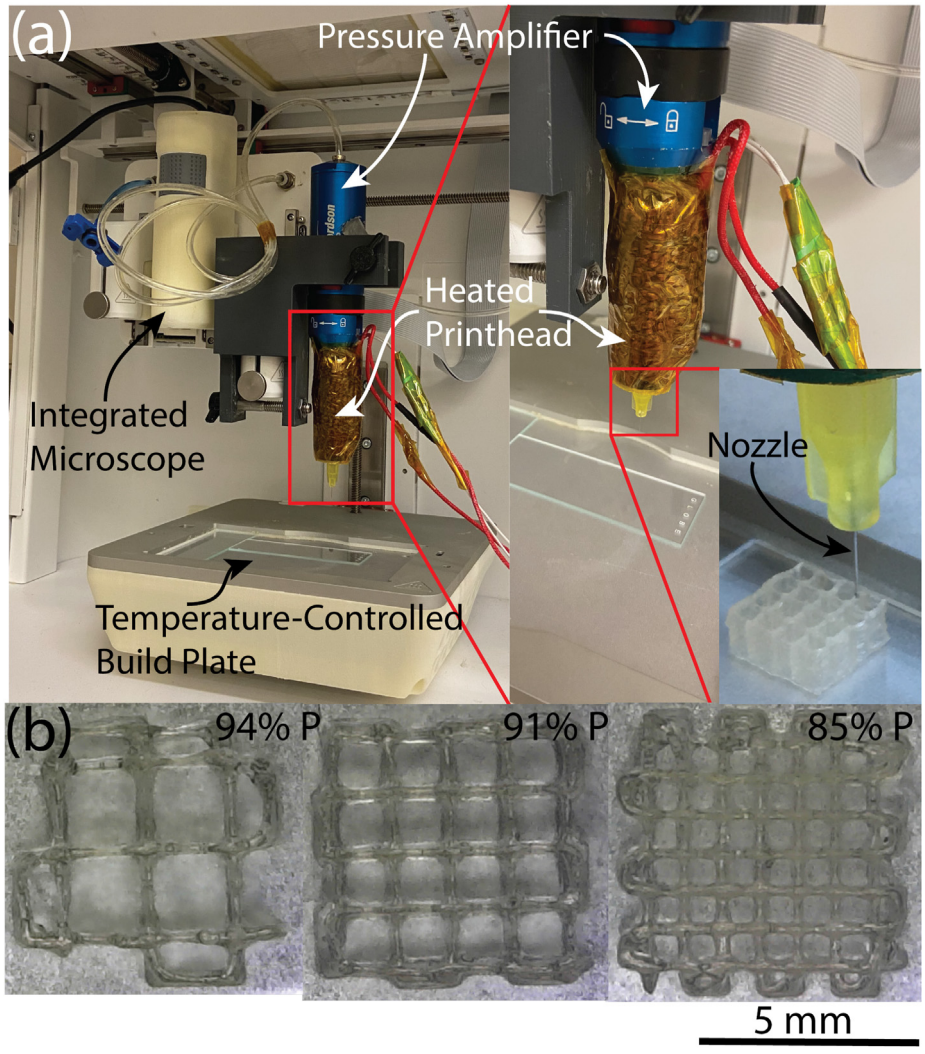

Fig. 2. (a) The modified BioX 3D printer with pressure amplifier, temperature controlled printhead and (b) 3D printed and crosslinked SA-GEL-GA scaffolds with varying porosities.

varied logarithmically between 0.1 and 100% at a constant frequency of 1 rad/s. Finally, to study the shear rate dependent stress and viscosity behavior of the hydrogels, flow ramp tests were performed at different temperatures where the rotational strain rate was varied between 1 and 600 s^{-1} in a logarithmically linear fashion over a 300 s period. Non-volatile mineral oil was applied around the cone and plate geometry for all the tests to prevent the hydrogels from drying during the experiment.

2.4. Fabrication of the scaffolds

The scaffolds were fabricated using a customized commercial BioX 3D Bioprinter (Cellink, Gothenburg, Sweden) as shown in Fig. 2(a). The 3D printer was modified with a pressure amplifier (Nordson HP3cc, Nordson Corp, Westlake, OH) that allows for a 7-fold pressure amplification to achieve a maximum effective pressure of 1400 kPa. The pressure amplifier head was combined with a cylindrical cartridge heater and a thermistor that are commonly used in commercial 3D printers and wrapped with insulating material. These devices were used in conjunction with a microcontroller system to control the printhead temperature in closed-loop to realize printing temperatures up to 100 °C. Porous scaffolds with a height of 2 mm in a 7.5 × 7.5 mm square pattern were fabricated with three different grid sizes as shown in Fig. 2(b). These geometries were obtained by slicing the rectangular prism-shaped part designs using different porosities, between 94% and 85%, and without any solid shell using the open source Slic3r slicing software. The porosity of a given scaffold is given as the ratio of the void volume to the total volume of the rectangular prism that encapsulates the scaffold.

Metal nozzles with a diameter of 100 μm (Part# 7018462, Nordson Corp, Westlake, OH) were used to extrude the hydrogels at a dispensing pressure of 630 kPa, printing speed of 7 mm/s. To study the effect of ink temperature on the printed scaffold geometry, we performed experiments with printhead temperatures of 35, 40 and 55 °C and printbed temperatures of 9,13,17 and 21 °C. These temperature levels were informed through the rheological characterization results given in Section 3.1.

2.5. Crosslinking of scaffolds

Upon 3D printing, the scaffolds were crosslinked both physically and chemically to achieve final mechanical properties and stability. Physical crosslinking of GEL was achieved by keeping the scaffolds in the fridge (nominally 4–8 °C as indicated by the fridge specifications) during the two subsequent chemical crosslinking steps. For the ionic crosslinking step, the scaffolds were immersed in an aqueous solution including 102 mM $CaCl_2$, and 5 mM HEPES at a pH of 7.4 to realize ionic cross-linking between SA and GA [24]. The scaffolds were then washed with DIW and immersed in a solution of 1 wt% EDC and 0.25 wt% NHS in the fridge to realize covalent cross-linking of GEL, GA, and SA [23]. The durations of the different chemical crosslinking steps were varied to understand their influences on the mechanical properties and degradation behavior of the scaffolds. Specifically, ionic cross-linking durations of 1, 4 and 7 h, and covalent cross-linking durations of 1, 4, 7, 15, 24, 48 and 72 h were tested. Following crosslinking, the scaffolds were washed with and stored in DIW to prevent dehydration until use in further studies.

2.6. Mechanical testing

Scaffolds with 94, 91 and 85% porosities, subjected to varying cross-linking durations as listed in Section 2.5 were tested to characterize their compressive elastic moduli. Prior to mechanical testing, all scaffolds were filled with 10% w/w GEL solution to mimic the cell-laden hydrogel that the structural scaffold is intended to support. The 10% gelatin filling was prepared by dissolving gelatin in DIW at 55 °C by continuous stirring with the high-speed mixer following the same protocols given in Section 2.2. The gelatin-filled scaffolds were incubated in the fridge for 30 min to allow for the physical crosslinking of gelatin. All scaffolds were prepared immediately prior to the mechanical testing to avoid any possible degradation prior to the test. Unconfined compression of the samples was achieved using an ARES G2 Rheometer (TA Instruments, New Castle, DE, USA) equipped with a normal transducer that has a range of 0.001–20 N. For the unconfined compression, two 25 mm diameter parallel flat aluminum plates were used. Samples were immersed in PBS inside a 100 mm Petri dish and allowed to equilibrate for 1 min at room temperature before testing.

The testing protocol began with measurement of the initial uncompressed thickness of each sample for accurate calculation of compressive strains and incorporating sample to sample variation in geometry. To this end, prior to placement of the sample in the test setup, the moving top plate was brought into contact with the bottom plate and the top plate position was zeroed. Next, the sample was introduced to the setup and the top plate was incrementally lowered towards the sample until a non-zero force reading was obtained, indicating the contact between the top plate and the sample. The vertical position of the top plate was then recorded as the initial sample thickness. The strain during the compressive test was then calculated by dividing the top plate displacement by this initial thickness. At the beginning of the compressive test, a sample preconditioning step was utilized to eliminate viscoelastic transient effects with a 3% compressive strain at a rate of 0.4% s^{-1}. Samples were kept at this strain for 100 s to achieve equilibration of elastic stress, monitored through the compressive force, and compressed with another 10% strain at a rate of 0.1% s^{-1}. The slope of the stress-strain data in this last step was used to determine the compressive modulus of the scaffold. To calculate the engineering stress, the force data obtained during this process was divided by the initial cross-sectional area of the sample, which was individually measured for each sample through microscopy images to account for sample-to-sample variations.

2.7. Swelling ratio and rehydration kinetics

To assess the swelling ratio of the 3D printed scaffolds, the scaffolds were weighed after crosslinking and dehydrated overnight in air under a hood at RT then weighed after dehydration. The swelling ratio was calculated according to

$$Swelling\ Ratio = \frac{W_s - W_d}{W_d} \times 100\%$$

Where W_s is the swollen scaffold's weight, and W_d is the dried scaffold's weight.

Rehydration kinetics were studied by rehydrating the dried scaffolds in DIW at room temperature and measuring the weight every 10 min for a total of 50 min a time at which no further swelling occurred based on prior weight vs. time measurements. The rehydration ratio was then calculated using the same formula and replacing the swollen weight with the rehydrated weight.

2.8. Scaffold degradation

To study scaffolds' degradation behavior, 3D printed and cross-linked scaffolds were lyophilized using a Labconco (Labconco Inc, Kansas City, MO) 2.5L, −55 °C freeze dryer where the vacuum was set to 0.033 mbar until the temperature decreased to −50 °C. The freeze dryer has an end-point detection system with an alert that compares the vacuum in the sample to a reference vacuum on an empty vessel. All samples were lyophilized for 24 h for consistency even after an end-point was detected. All samples were weighed on day 0. Samples were then put in individual 15 ml centrifuge tubes and covered with 2 ml base medium consisting of DMEM/F-12 supplemented with 10% FBS and 1% antibiotic antimycotic, and incubated with gentle 175 rpm shaking at 37 °C in a Thermo Scientific MaxQ 4450 shaker (Thermofisher Scientific, Waltham, MA). Every other day, the samples were gently dried with a napkin to absorb

the excess medium weighed, placed in fresh medium. At the end of the study, final weights were determined.

2.9. Statistical analysis

Statistical significance was determined between groups using an independent Student's t-test using GraphPad Prism (GraphPad Software, San Diego, CA). Data are represented as mean ± standard error of the mean (SEM), and a P value of <0.05 was considered statistically significant.

3. Results and discussion

3.1. Hydrogel rheology and 3D printing

Rheology of a given ink plays a critical role in determining its processability through additive manufacturing operations. The results of the rheological characterization are presented in Fig. 3. At temperatures below ~28 °C, the inks exhibit the rheological nature of an elastic solid rather than a viscous liquid (Elastic Modulus (G′)»Viscous Modulus (G″)) as shown in Fig. 3(a) with no distinct yielding under about 1 kPa stress, as indicated by a lack of a clear intersection of G′ and G″ curves in Fig. 3(b). At all temperatures above 28 °C, a nearly constant tan δ (ratio of G''/G') was observed. This behavior is reminiscent of the sol-gel transition reported for GEL [25] and GEL-SA mixtures [26] that occur between 25 and 30 °C. However, unlike GEL or GEL-SA, the tan δ value for the SA-GEL-GA hydrogel does not exceed a value of 1 at high temperatures, indicating elastic effects narrowly exceed the viscous effects in the ink behavior. Inclusion of GA induces this behavior which is deemed favorable for extrusion-based 3D printing applications in general [27]. Above 28 °C, the hydrogel exhibits significantly lower yield stresses compared to those observed at lower temperatures as shown in Fig. 3(b). The flow ramp data in Fig. 3(c) shows that the hydrogel behavior at these temperatures can be represented by the Herschel-Bulkley model [28], characterized by a yield stress (rate independent constant stress at low shear rates) and shear thinning nature ($n < 1$) at high strain rates. Even though the yield stress does not show significant temperature dependence above 28 °C, hydrogel viscosity decreases with increasing temperature as shown in Fig. 3(d).

These results provide critical insights regarding the temperature control of the SA-GEL-GA hydrogel during the printing process. First, the hydrogel needs to be heated above 28 °C prior to extrusion since below this temperature, large yield stresses need to be overcome to shear the hydrogel without initiating plug flow caused by the slip between the material and the nozzle wall [29]. In fact, we observed that the hydrogel can be extruded at pressures lower than those needed to induce yield stresses, i.e. > 1 kPa, at the particular flow rates observed, which offers a strong evidence of such undesired plug flow effects. As such, we utilize the heated print head to increase hydrogel temperature to reduce hydrogel viscosity and yield stress, and achieve shear thinning which is critical for extrusion-based AM applications [30]. It should be noted that the low yield stresses observed at higher temperatures do not necessarily mean that low dispensing pressures commensurate with the yield stresses will be sufficient for optimal printing. This is exemplified by the fact that a pressure of 630 kPa was required in our experiments at high printhead temperatures. This is due to the fact that the majority of the pressure energy is needed to overcome (1) the internal friction due to material viscosity that occurs during shear flow at a particular flow rate inside the printing nozzle, and (2) energy losses at the sudden contraction at the nozzle entry, both of which increase dramatically with increasing flow speed [31].

Following the extrusion of the hydrogels, shape retention of the deposited filaments requires low tan δ value (i.e. Elastic Modulus (G')»Viscous Modulus (G″) thus elastic effects dominating the viscous effects), to prevent spreading and loss of accuracy. Such behavior is observed at lower temperatures, which is why the use of a cooled substrate surface was deemed necessary. Printhead and substrate temperatures for optimal printing should be selected such that the hydrogels are heated to a high enough temperature to achieve sufficiently low viscosity for extrusion, and the substrate should be cooled to a low enough temperature to quickly "gelate" the hydrogel to retain proper shape after printing. It should be noted that this is an optimization problem, since higher printhead temperatures would necessitate lower substrate temperatures, to cool down and "lock in" the shape of the printed filaments prior to their spreading.

To study the influence of substrate temperature on the printing

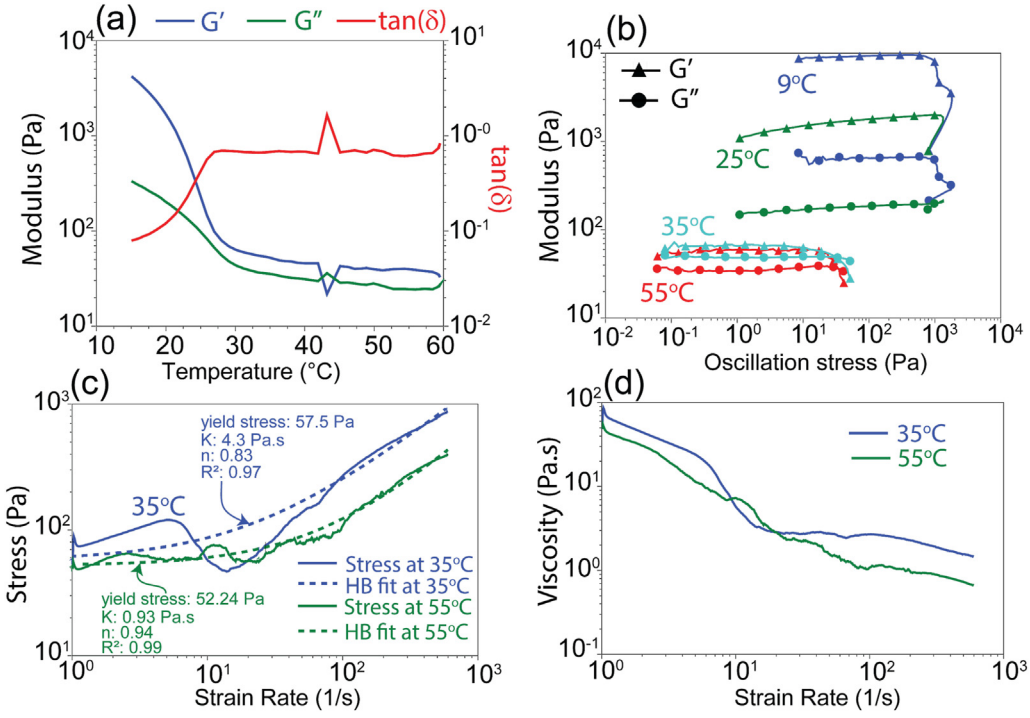

Fig. 3. Temperature dependent rheological characteristics of the SA-GEL-GA hydrogel (a) Oscillatory temperature sweep test showing a "gelation-like" behavior below ~28 °C (sharp variation around 43 °C is an experimental aberration due to equipment error), (b) Oscillatory amplitude sweep test indicating high yield stresses for the inks at low temperatures, (c) Flow ramp tests along with Herschel-Bulkley (HB) model fits, indicating the presence a yield stress and shear thinning behavior as well as (d) reduction of the viscosity with increasing temperature.

process, we kept the printhead temperature at 55 °C and varied the substrate temperature. As shown in Fig. 4, printability reduces with increasing substrate temperature. An average deposited filament diameter of 250 μm is achieved at substrate temperatures below 13 °C, but this diameter almost doubled at 21 °C at constant printing speed and dispensing pressure due to excessive spreading of the filament. The prints consistently failed under ambient conditions (no substrate cooling).

Fig. 5 shows the results of the study on the influence of printhead temperature on the printing process. During these experiments, the printhead temperature was varied between 35 and 55 °C while keeping the substrate temperature at 9 °C and the dispensing pressure at 630 kPa. To evaluate the repeatability of scaffold quality, three replicates for each case are presented. As shown, the occurrence of printing defects increases with decreasing temperatures and consistency of the prints is reduced. In the remainder of the experiments presented in this work, to maximize the scaffold quality for further studies, we used 55 °C and 9 °C as printhead and substrate temperatures, respectively. Using these parameters, we were able to extrude SA-GEL-GA from 100 μm diameter nozzles and obtain high fidelity scaffolds with printed filament diameter as small as 250 μm through high temperature extrusion onto cooled substrates as shown in Figs. 2, 4 and 5. These dimensions constitute an improvement in bioprinting resolution over GEL and SA type gels, without using support gels [32] or nanoparticle based rheological modifiers [15,33] which limit the use of small nozzles due to excessive clogging. It should be noted that for applications involving living cells in the printed constructs, such high printhead temperatures are likely to be detrimental. In such applications, printing near or below physiological temperatures is required. The results presented here indicate that, despite this sub-optimal quality, the SA-GEL-GA hydrogel can be printed at physiological temperatures, highlighting its potential for cell-laden printing applications.

3.2. Mechanical properties of SA-GEL-GA scaffolds

We studied the influence of three factors on the compressive mechanical properties of the scaffolds printed using the SA-GEL-GA hydrogels, porosity, crosslinking duration in NHS-EDC and crosslinking duration in $CaCl_2$. The compressive elastic moduli of the scaffolds with three porosities of 94%, 91%, and 85% are presented in Fig. 6(a). These samples were crosslinked for 1 h each in $CaCl_2$ and NHS-EDC prior to filling, and three replicates for each sample were created. As shown in Fig. 6(a), the moduli increased as the porosity decreased, the individual values were 48.4 ± 6.9 kPa, 109.1 ± 4.7 kPa, and 169.5 ± 3.8 kPa corresponding to porosities of 94%, 91%, and 85%, respectively. These values are substantially higher by 3–10 times over those estimated for the pure gelatin sample with the same geometry but without any SA-GEL-GA scaffold which yielded an elastic modulus of a mere 17.8 ± 1.0 kPa. This result shows that SA-GEL-GA can be used to fabricate structural scaffolds providing mechanical support to artificial tissues, the degree to which can be controlled through the scaffold design, particularly the porosity, i.e., the grid spacing or size. It should be noted that variation of the grid size of the acellular scaffolds has other implications besides the impact on mechanical properties. Most importantly, reduction in grid size means lower cell density as the cell-containing portions of the scaffolds will occupy a lower proportion of the overall construct. As such, methods for controlling mechanical properties without varying the scaffold design should be explored.

Fig. 6(b) shows the variation of the compressive modulus with crosslinking duration in NHS-EDC. These samples have a porosity of 91% and were crosslinked in $CaCl_2$ for 1 h prior to NHS-EDC crosslinking and GEL filling. As shown, the compressive moduli increased with increasing NHS-EDC crosslinking duration up to 24 h. No significant change was observed between 24 and 48 h, whereas a more than 50% decrease in the compressive modulus was observed when the cross-linking duration was extended to 72 h. The individual values of the data points given in Fig. 6(b) were: 109.1 ± 4.7 kPa, 152.5 ± 4.7 kPa, 173 ± 9.4 kPa, 237.6 ± 22 kPa, 238.5 ± 4.4 kPa, and 123.6 ± 41.3 kPa, corresponding to 1 h, 4 h, 7 h, 24 h, 48 h, and 72 h NHS-EDC crosslinking duration, respectively. These results indicate that the mechanical properties of the crosslinked SA-GEL-GA scaffolds can be controlled by tuning the covalent bond density between the amine groups in GEL and the carboxylic groups in SA, GA, and GEL through NHS-EDC immersion duration within 24 h. The modulus not changing between 24 and 48 h of crosslinking might be attributed to multiple reasons. The maximum allowable covalent crosslink density may have been achieved within the first day. Alternatively, it is known that the stability of the NHS-EDC solution is reduced one day after preparation [34]. The significant reduction in modulus on the third day indicates degradation of the scaffolds within the unstable NHS-EDC solution. Further analysis of this effect is beyond the scope of this paper.

Fig. 6(c) shows the variation of the compressive modulus with crosslinking duration in the $CaCl_2$ solution. These samples had a porosity of 91% and were crosslinked in NHS-EDC for 1 h following the $CaCl_2$ crosslinking. As shown in Fig. 6 (c), increasing the $CaCl_2$ cross-linking duration led to a slight decrease in the mechanical properties. Their individual values were 109.1 ± 4.7 kPa, 95.7 ± 4.5 kPa, and 95.1 ± 0.7 kPa, corresponding to 1 h, 4 h, and 7 h $CaCl_2$ crosslinking duration, respectively. This result indicates that optimal ionic crosslinking is achieved within the first hour. Further $CaCl_2$ immersion acts adversely, due to saturation of the carboxylic groups in Gelatin with Ca^{2+} ions which in turn impedes the ability of the NHS-EDC to activate these for improved covalent bonding with amine groups [35].

The demonstrated capability of controlling the compressive modulus through the cross-linking process introduces a new degree of freedom in bio-printed scaffold design and mechanical property control, specifically enabling varying mechanical properties without varying the scaffold grid size or filament diameter. The demonstrated compressive modulus range of 50–250 kPa is well suited for biomimicking of skin properties [4]. It should be noted that a large parameter space including different nozzle sizes and crosslinking duration-porosity combinations remain unexplored and such information can serve to broaden the property range and application domains. It is evident from the results that a compressive modulus of over 250 kPa is achievable with a porosity 85% and a cross-linking duration of 24 h.

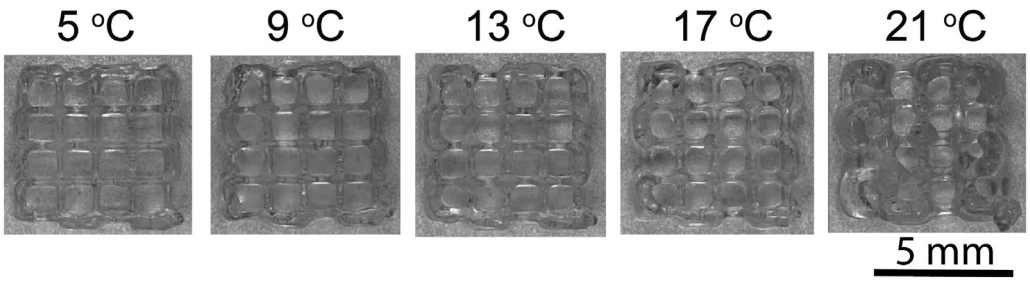

Fig. 4. Scaffolds printed at varying substrate temperatures indicating the decrease in printability with increasing substrate temperature.

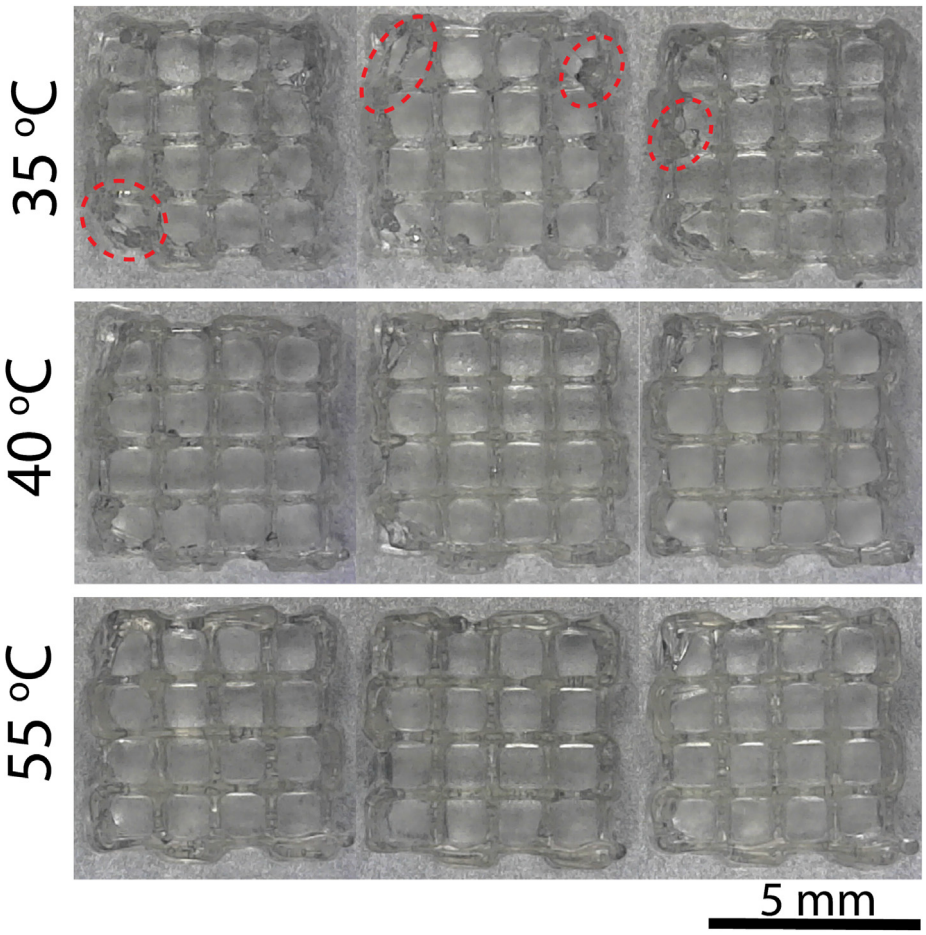

Fig. 5. Scaffolds printed using different printhead temperatures. Three repetitions for each temperature are shown. Several defects are highlighted with dashed red ellipses. (For interpretation of the references to colour in this figure legend, the reader is referred to the Web version of this article.)

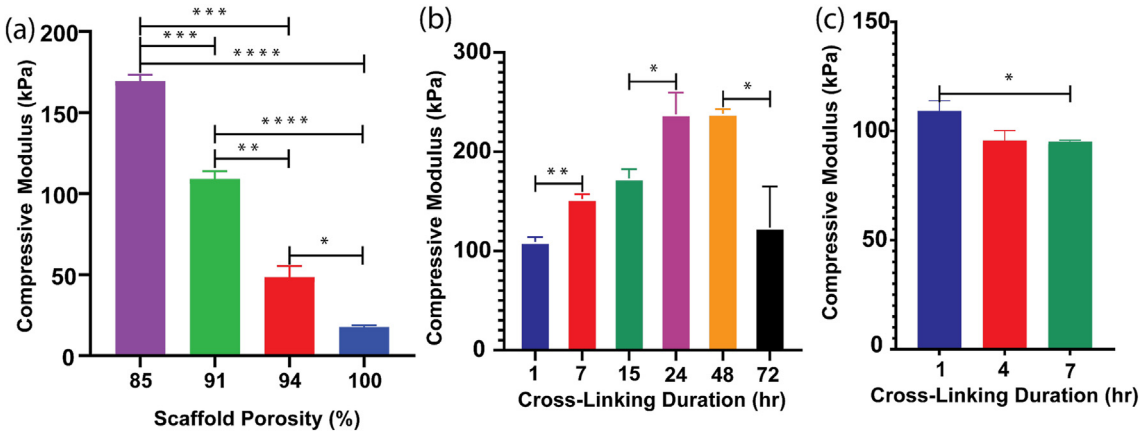

Fig. 6. Variation of compressive elastic modulus of the SA-GEL-GA scaffolds filled with 10% gelatin: (a) influence of scaffold porosity, (b) influence of cross-linking duration in NHS-EDC, and (c) influence of cross-linking duration in $CaCl_2$. (Mean ± SEM, n = 3, *P < 0.05, **P < 0.01, ***P < 0.001, ****P < 0.0001).

3.3. Swelling ratio and rehydration kinetics

For tissue scaffolding hydrogels, the capability of retaining water is critical, as it has many implications on hydrogel performance, such as allowing nutrient diffusion to the cells as well as waste exudation [36]. Moreover, most native tissues exhibit viscoelastic behavior critical to their functionality, primarily owing to their water content. For instance, for articular cartilage as well as biomimicking hydrogels, increasing amounts of water imbibed into the tissues have been shown to increase load-bearing capability [37]. To determine how much water the scaffolds carry right after printing and crosslinking, the swelling ratio for the crosslinked 3D printed scaffolds was determined through the ratio of mass in freshly crosslinked (and saturated with water) and dried states, as detailed in the methods section, and summarized in Fig. 7(a) as a function of porosity. As shown, no significant differences were detected for porosities in the 85% – 91% range, with an average swelling ratio of

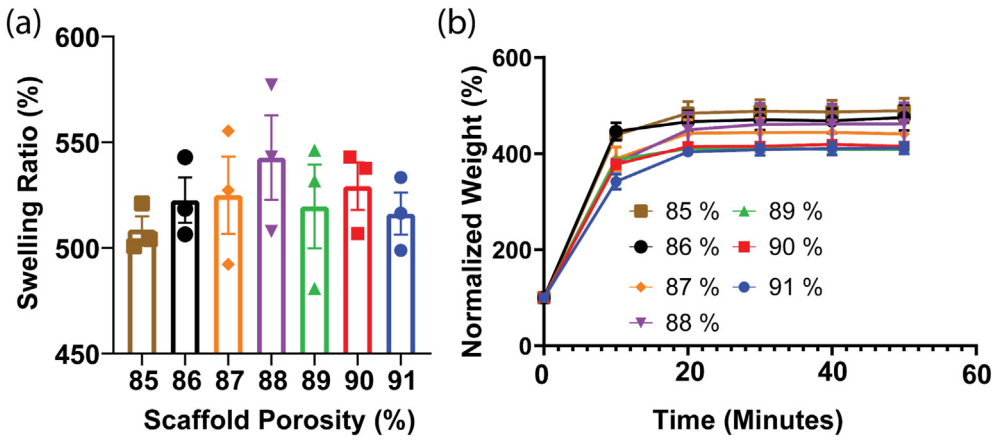

Fig. 7. Results of the swelling ratio and rehydration kinetics analyses: (a) Swelling ratio of 3D-printed and cross-linked hydrogels with varied scaffold porosities, and (b) Rehydration kinetics for crosslinked 3D-printed scaffolds after dehydration overnight and rehydration for 50 min (Mean ± SEM, n = 3).

523%, indicating that the SA-GEL-GA hydrogels can carry over 5 times their dry weight in water. This result demonstrates the potential of SA-GEL-GA hydrogel use for fabricating scaffolds that can carry and support living cells and other biomaterials.

We also studied the rehydration kinetics of SA-GEL-GA to assess the capability of rehydrating to a swollen state from a completely dried state, a quality needed for long-term storage and transportation. In these experiments, we studied the influence of porosity on the rehydration rate and the total amount of water that can be reintroduced to the scaffolds, with the results given in Fig. 7(b). All scaffolds were fully rehydrated after 10 min, with no significant differences in average rehydration rate between the different porosities. The scaffolds rehydrated to about 400% or more of their dry weight which is consistently around 25% less than their swelling ratio for all porosities. It was observed that the scaffolds with lower porosities were able to regain up to 25% more water. Considering the main mechanism of reswelling is diffusion, this result is likely due to the increased total surface area to volume ratio in the scaffolds with lower porosities, particularly at layer-to-layer interfaces between the printed filaments. In general, the high level of reswelling capability of SA-GEL-GA reduces or eliminates the need for acellular scaffolds to be kept hydrated prior to infusion with cells, during transportation or long-term storage.

3.4. Degradation and long-term stability

The degradation or stability of the 3D printed scaffolds under cell culture conditions is a critical parameter for determining capability in supporting cell culture *in vitro*. Here, we studied the degradation characteristics of the SA-GEL-GA hydrogels in culture medium. We particularly focused on the influence of NHS-EDC crosslinking duration, as it has been shown to significantly affect the mechanical properties of the scaffolds. Specifically, three durations (1 h, 12 h, and 24 h) were studied. The results of the analyses are shown in Fig. 8. Scaffolds crosslinked for 1 h in NHS-EDC maintained their mass for 23 days without significant weight loss. The 12 h crosslinked scaffolds showed rapid degradation after 21 days (Fig. 8(a)) with an average and statistically significant weight loss between Day 2 and 23 of 10%. The 24 h crosslinked scaffolds lost a substantial 22% mass loss with a marked decrease beginning at Day 16 continuing through Day 23. We observed that these scaffolds began to mechanically fail by separating at several layer interfaces after day 16. We recovered the separated layers and weighed them together to produce the data given in Fig. 8 (a). As such, it is likely that at least a part of the mass loss can be attributed to the loss of small segments of material that cannot be recovered from the medium. This result indicates that highly covalently cross-linked scaffolds exhibit brittle behavior leading to reduced long-term stability, as a trade-off with their increased compressive modulus. This finding should be taken in context since the presented degradation tests were performed using a bare porous scaffold without a supporting matrix, likely inducing a more rapid degradation behavior compared to practical application cases.

4. Conclusions

Our results show that the SA-GEL-GA hydrogels present promising

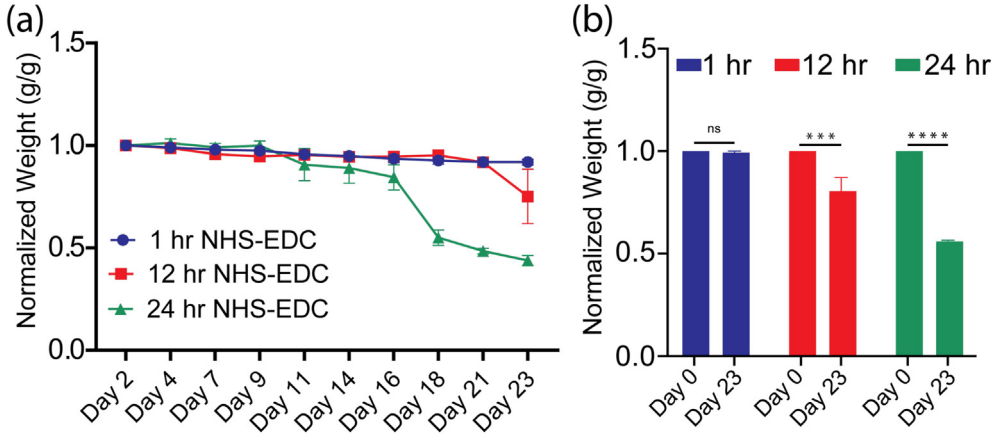

Fig. 8. Long term degradation and stability analysis of hydrogels as a function of varying cross-linking durations in NHS-EDC: (a) Variation of scaffold mass during the testing normalized with respect to Day 2, and (b) Variation of lyophilized scaffold weight in 23 days, normalized with respect to Day 0. (Mean ± SEM, n = 3, ns $P > 0.05$, ***$P < 0.001$, ****$P < 0.0001$).

potential for 3D printed scaffolds, by offering improved printing resolution and a higher level of control of mechanical properties, thus enabling more accurate mimicking of native tissue properties compared to many conventional hydrogels used in bioprinting applications. These advantages are complimented by SA-GEL-GA's capability of carrying over 5 times its gel weight in water and reswell to over 4 times its weight, providing promise for effective utilization in tissue engineering applications. It should be noted that the parameter space explored in this work, particularly the extrusion temperature, nozzle diameter and crosslinking times, is tailored for an acellular application of the hydrogels. In such an application, the cells would be seeded onto or encapsulated in another hydrogel and combined with SA-GEL-GA scaffolds. Our preliminary results on compatibility of the SA-GEL-GA with bovine chondrocytes for such an application are provided in the Supporting Information section S1. For an application where the cells are encapsulated in SA-GEL-GA and printed, larger nozzles and lower dispensing pressures thereby inducing lower shear stresses on the cells, along with printing temperatures at or below physiological levels will be required. Finally, cytotoxicity of the cross-linking process, particularly for the long duration covalent cross-linking cases should be studied. Our results indicate that SA-GEL-GA can be printed at physiological temperatures. Furthermore, our preliminary studies showed that a crosslinking process with 1 h immersion in NHS-EDC did not lead to any noticeable cell-viability issues (see Supporting Information Section S2). A more detailed analysis of cell-laden printing of SA-GEL-GA will be performed as a part of our future work.

In addition to the cell-laden application of SA-GEL-GA, our future plans also involve investigating various means of increasing the achievable mechanical property range by studying how hydrogel composition, particularly the relative concentrations of SA, GA and GEL, influences the final mechanical properties, swelling and rehydration behavior and, long-term stability. Finally, we will study the influence of several printing parameters such as printing speed, dispensing pressure, and printhead and substrate temperatures on the final properties of printed scaffolds. Such parameters have been shown to influence microstructure, particularly of multi-component bioinks [38], which can in turn affect functional properties.

Funding statement

This work was financially supported by the National Science Foundation grants 1606226 and 1658845, and start-up funds for co-author Nehal Abu-Lail from the University of Texas- San Antonio.

CRediT authorship contribution statement

Mahmoud Amr: Conceptualization, Methodology, Validation, Formal analysis, Investigation, Data curation, Writing – original draft, Visualization, Supervision. **India Dykes:** Methodology, Formal analysis, Investigation, Data curation, Writing – review & editing. **Michele Counts:** Methodology, Investigation, Writing – review & editing. **Joshua Kernan:** Methodology, Investigation, Writing – review & editing. **Alia Mallah:** Methodology, Investigation, Writing – review & editing. **Juana Mendenhall:** Writing – review & editing, Supervision, Funding acquisition. **Bernard Van Wie:** Writing – review & editing, Supervision, Funding acquisition. **Nehal Abu-Lail:** Writing – review & editing, Supervision, Funding acquisition. **B. Arda Gozen:** Conceptualization, Methodology, Formal analysis, Investigation, Data curation, Writing – original draft, Visualization, Supervision, Project administration, Funding acquisition.

Declaration of competing interest

The authors declare that they have no known competing financial interests or personal relationships that could have appeared to influence the work reported in this paper.

References

[1] X. Ma, J. Liu, W. Zhu, M. Tang, N. Lawrence, C. Yu, M. Gou, S. Chen, 3D bioprinting of functional tissue models for personalized drug screening and in vitro disease modeling, Adv. Drug Deliv. Rev. 132 (2018) 235–251.
[2] I.T. Ozbolat, M. Hospodiuk, Current advances and future perspectives in extrusion-based bioprinting, Biomaterials 76 (2016) 321–343.
[3] P.G. Agache, C. Monneur, J.L. Leveque, J. De Rigal, Mechanical properties and young's modulus of human skin in vivo, Arch. Dermatol. Res. 269 (2008) 221–232.
[4] C. Li, G. Guan, R. Reif, Z. Huang, R.K. Wang, Determining elastic properties of skin by measuring surface waves from an impulse mechanical stimulus using phase-sensitive optical coherence tomography, J. R. Soc. Interface 9 (2012) 831–841.
[5] J.Y. Rho, R.B. Ashman, C.H. Turner, Young's modulus of trabecular and cortical bone material: ultrasonic and microtensile measurements, J. Biomech. 26 (1993) 111–119.
[6] R. Raghupathy, C. Witzenburg, S.P. Lake, E.A. Sander, V.H. Barocas, Identification of regional mechanical anisotropy in soft tissue analogs, J. Biomech. Eng. 133 (2011).
[7] W.M. Han, S.J. Heo, T.P. Driscoll, M.E. Boggs, R.L. Duncan, R.L. Mauck, D.M. Elliott, Impact of cellular microenvironment and mechanical perturbation on calcium signalling in meniscus fibrochondrocytes, Eur. Cell. Mater. 27 (2014) 321–331.
[8] S.J. Mousavi, M. Hamdy Doweidar, Role of mechanical cues in cell differentiation and proliferation: a 3D numerical model, PloS One 10 (2015) 1–23.
[9] B.A.G.G. de Melo, Y.A. Jodat, S. Mehrotra, M.A. Calabrese, T. Kamperman, B.B. Mandal, M.H.A.A. Santana, E. Alsberg, J. Leijten, S.R. Shin, 3D printed cartilage-like tissue constructs with spatially controlled mechanical properties, Adv. Funct. Mater. 29 (2019) 1–13.
[10] W. Schuurman, V. Khristov, M.W. Pot, P.R. van Weeren, W.J. a Dhert, J. Malda, Bioprinting of hybrid tissue constructs with tailorable mechanical properties, Biofabrication 3 (2011), 021001.
[11] J. Kundu, J.H. Shim, J. Jang, S.W. Kim, D.W. Cho, An additive manufacturing-based PCL-alginate-chondrocyte bioprinted scaffold for cartilage tissue engineering, J. Tissue Eng. Regen. Med. 11 (2015) 1286–1297.
[12] J.H.Y.Y. Chung, J.C. Kade, A. Jeiranikhameneh, K. Ruberu, P. Mukherjee, Z. Yue, G.G. Wallace, 3D hybrid printing platform for auricular cartilage reconstruction, Biomed, Phys. Eng. Express 6 (2020), 035003.
[13] J. Visser, F.P.W.W. Melchels, J.E. Jeon, E.M. Van Bussel, L.S. Kimpton, H.M. Byrne, W.J.A.A. Dhert, P.D. Dalton, D.W. Hutmacher, J. Malda, Reinforcement of hydrogels using three-dimensionally printed microfibres, Nat. Commun. 6 (2015) 1–10.
[14] J.S. Dounchis, R.D. Coutts, D. Amiel, Cartilage repair with autogenic perichondrium cell/polylactic acid grafts: a two-year study in rabbits, J. Orthop. Res. 18 (2000) 512–515.
[15] Y. Jin, C. Liu, W. Chai, A. Compaan, Y. Huang, Self-supporting nanoclay as internal scaffold material for direct printing of soft hydrogel composite structures in air, ACS Appl. Mater. Interfaces 9 (2017) 17456–17465.
[16] S.J. Kalita, S. Bose, H.L. Hosick, A. Bandyopadhyay, Development of controlled porosity polymer-ceramic composite scaffolds via fused deposition modeling, Mater. Sci. Eng. C 23 (2003) 611–620.
[17] S.M. Bittner, B.T. Smith, L. Diaz-Gomez, C.D. Hudgins, A.J. Melchiorri, D.W. Scott, J.P. Fisher, A.G. Mikos, Fabrication and mechanical characterization of 3D printed vertical uniform and gradient scaffolds for bone and osteochondral tissue engineering, Acta Biomater. 90 (2019) 37–48.
[18] M. Castilho, V. Mouser, M. Chen, J. Malda, K. Ito, Bi-layered micro-fibre reinforced hydrogels for articular cartilage regeneration, Acta Biomater. 95 (2019) 297–306.
[19] O. Bas, S. Lucarotti, D.D. Angella, N.J. Castro, C. Meinert, F.M. Wunner, E. Rank, G. Vozzi, T.J. Klein, I. Catelas, E.M. De-Juan-Pardo, D.W. Hutmacher, Rational design and fabrication of multiphasic soft network composites for tissue engineering articular cartilage: a numerical model-based approach, Chem. Eng. J. 340 (2018) 15–23.
[20] R. Schipani, D.R. Nolan, C. Lally, D.J. Kelly, Integrating finite element modelling and 3D printing to engineer biomimetic polymeric scaffolds for tissue engineering, Connect. Tissue Res. 61 (2020) 174–189.
[21] R. Schipani, S. Scheurer, R. Florentin, S.E. Critchley, D.J. Kelly, Reinforcing interpenetrating network hydrogels with 3D printed polymer networks to engineer cartilage mimetic composites, Biofabrication 12 (2020), 035011.
[22] M. Castilho, G. Hochleitner, W. Wouter, B. Van Rietbergen, D. Paul, Mechanical Behavior of a Soft Hydrogel Reinforced with Three- Dimensional Printed Microfibre Scaffolds, 2018, pp. 1–10.
[23] L. Shi, L. Xiong, Y. Hu, W. Li, Z.C. Chen, K. Liu, X. Zhang, Three-dimensional printing alginate/gelatin scaffolds as dermal substitutes for skin tissue engineering, Polym. Eng. Sci. 58 (2018) 1782–1790.
[24] M. Li, H. Li, X. Li, H. Zhu, Z. Xu, L. Liu, J. Ma, M. Zhang, A bioinspired alginate-gum Arabic hydrogel with micro-/nanoscale structures for controlled drug release in chronic wound healing, ACS Appl. Mater. Interfaces 9 (2017) 22160–22175.
[25] H.B. Bohidar, S.S. Jena, Kinetics of sol-gel transition in thermoreversible gelation of gelatin, J. Chem. Phys. 98 (1993) 8970–8977.
[26] T.B. Goudoulas, N. Germann, Phase transition kinetics and rheology of gelatin-alginate mixtures, Food Hydrocolloids 66 (2017) 49–60.
[27] J.a. Lewis, Direct ink writing of 3D functional materials, Adv. Funct. Mater. 16 (2006) 2193–2204.
[28] H.S. Tang, D.M. Kalyon, Estimation of the parameters of Herschel-Bulkley fluid under wall slip using a combination of capillary and squeeze flow viscometers, Rheol. Acta 43 (2004) 80–88.
[29] G. Siqueira, D. Kokkinis, R. Libanori, M.K. Hausmann, A.S. Gladman, A. Neels, P. Tingaut, T. Zimmermann, J.A. Lewis, A.R. Studart, Cellulose nanocrystal inks for

3D printing of textured cellular architectures, Adv. Funct. Mater. 27 (2017) 1604619.
[30] J.T. Muth, D.M. Vogt, R.L. Truby, Y. Mengüç, D.B. Kolesky, R.J. Wood, J.a. Lewis, Embedded 3D printing of strain sensors within highly stretchable elastomers, Adv. Mater. 26 (2014) 6307–6631.
[31] G.M. Eccleston, N.E. Hudson, The use of a capillary rheometer to determine the shear and extensional flow behaviour of nasal spray suspensions, J. Pharm. Pharmacol. 52 (2000) 1223–1232.
[32] Y. Jin, W. Chai, Y. Huang, Printability study of hydrogel solution extrusion in nanoclay yield-stress bath during printing-then-gelation biofabrication, Mater. Sci. Eng. C 80 (2017) 313–325.
[33] K. Markstedt, A. Mantas, I. Tournier, H. Martínez Ávila, D. Hägg, P. Gatenholm, 3D bioprinting human chondrocytes with nanocellulose-alginate bioink for cartilage tissue engineering applications, Biomacromolecules 16 (2015) 1489–1496.
[34] N. Xia, Y. Xing, G. Wang, Q. Feng, Q. Chen, H. Feng, X. Sun, L. Liu, Probing of EDC/NHSS-mediated covalent coupling reaction by the immobilization of electrochemically active biomolecules, Int. J. Electrochem. Sci. 8 (2013) 2459–2467.
[35] Q. Xing, K. Yates, C. Vogt, Z. Qian, M.C. Frost, F. Zhao, Increasing mechanical strength of gelatin hydrogels by divalent metal ion removal, Sci. Rep. 4 (2014) 1–10.
[36] C. Ji, A. Khademhosseini, F. Dehghani, Enhancing cell penetration and proliferation in chitosan hydrogels for tissue engineering applications, Biomaterials 32 (2011) 9719–9729.
[37] F. Horkay, P.J. Basser, Composite hydrogel model of cartilage predicts its load-bearing ability, Sci. Rep. 10 (2020) 1–7.
[38] B.A. Nerger, P.T. Brun, C.M. Nelson, Microextrusion printing cell-laden networks of type i collagen with patterned fiber alignment and geometry, Soft Matter 15 (2019) 5728–5738.